

Understanding the multiwavelength observation of Geminga's TeV halo: the role of anisotropic diffusion of particles

Ruo-Yu Liu¹, Huirong Yan^{1,2}, and Heshou Zhang^{1,2}

¹*Deutsches Elektronen Synchrotron (DESY), Platanenallee 6, D-15738 Zeuthen, Germany*

²*Institut für Physik und Astronomie, Universität Potsdam, D-14476 Potsdam, Germany*

In this letter we demonstrate that the X-ray and the TeV observations in the vicinity of Geminga can be understood in the framework of anisotropic diffusion of injected electrons/positrons. This interpretation only requires the turbulence in the vicinity of Geminga to be sub-Alfvénic with the local mean magnetic field direction approximately aligned with our line of sight towards Geminga, without invoking extreme conditions for the environment, such as an extremely small diffusion coefficient and a weak magnetic field of strength $< 1\mu\text{G}$ as suggested in previous literature.

Introduction- The recent observation of the High-Altitude Water Cherenkov Observatory (HAWC) has revealed a TeV gamma-ray halo around the Geminga pulsar, with a spatial extension of $\gtrsim 30\text{ pc}$ [1]. The TeV emission is believed to arise from cosmic-ray electrons/positrons (hereafter we do not distinguish positrons from electrons unless specified) injected from the pulsar wind nebula (PWN), via inverse-Compton (IC) scattering off cosmic microwave background (CMB) photons. The detection of such a diffuse TeV emission has been interpreted as the presence of a slow diffusion zone around the pulsar [1–4] in the framework of 1D isotropic diffusion. Under the same framework, Ref.[5] studied the X-ray observation by XMM-Newton and Chandra in the vicinity of Geminga and an upper limit of $5 \times 10^{-15} \text{ erg cm}^{-2} \text{ s}^{-1}$ for the diffuse X-ray emission in $0.7 - 1.3 \text{ keV}$ has been obtained for a region within $600''$ around the pulsar. Since X-ray is supposed to arise from synchrotron radiation of the same electrons that account for the TeV emission observed by HAWC, the authors found that the X-ray upper limit, on the premise of fitting HAWC's observation, translates to an upper limit for the magnetic field strength in the TeV halo, i.e., $\leq 0.8\mu\text{G}$, which is significantly weaker than the typical interstellar medium (ISM) magnetic field. The combination of a small diffusion coefficient and a weak magnetic field would imply the saturation of the turbulence ($\delta B_g/B \simeq 1$ where δB_g is the fluctuation amplitude of magnetic field at the gyro-scale of particles and B is the mean magnetic field) and the Bohm limit of diffusion, which is, however, very difficult to achieve. For interstellar turbulence, the energy injection scale is $\sim 100\text{ pc}$ and much larger than the gyroscale of the TeV-emitting electrons, where the resonant scattering happens. It is unlikely that $\delta B_g/B$ approaches to unity. The only possibility is the small-scale waves generated by instabilities. The electron flux at 100 TeV is, nonetheless, too small to generate strong enough streaming instability to overcome Landau damping [6] as well as damping by the background turbulence [7–10].

Let us reconsider the theoretical interpretation from the perspective of the nature of the magnetic field in ISM:

it generally has a mean direction within one coherent length, which is typically $\sim 50 - 100\text{ pc}$ and comparable to the size of the TeV halo. 1D particle diffusion actually cannot hold in this scenario, since particles diffuse faster along the mean magnetic field than they diffuse perpendicular to the mean magnetic field in the case of sub-Alfvénic turbulence with the perpendicular diffusion coefficient being $D_\perp = D_\parallel M_A^4$, where D_\parallel is the diffusion coefficient parallel to the magnetic field, $M_A \equiv \delta B_{\text{inj}}/B$ is the Alfvénic Mach number, which is not far from unity for ISM (i.e., $M_A > 0.1$), and δB_{inj} is the magnetic perturbation at the injection scale of magnetohydrodynamic (MHD) turbulence or coherence length of magnetic field [11, 12]. Also, the synchrotron radiation intensity becomes anisotropic. Electrons that move along the magnetic field will radiate much less efficiently than those move perpendicular to the magnetic field. Therefore, if the mean magnetic field in the vicinity of Geminga has small inclination toward our line of sight (LOS), the observed synchrotron radiation flux would be much reduced compared to that with the assumption of an isotropic magnetic field, while the diffusion perpendicular to the LOS is slow as suggested by the TeV observation.

In this letter, we show that both X-ray and TeV observations can be explained with typical conditions for ISM, such as the magnetic field, the diffusion coefficient and the field perturbation level, by considering anisotropic particle diffusion which is a natural outcome in the presence of sub-Alfvénic turbulence. We will see that the viewing angle plays an important role in determining the observation signals.

Method- The temporal evolution of particle number density in space and energy space N is governed by the transport equation

$$\frac{\partial N}{\partial t} = \nabla \cdot (\mathcal{D} \cdot \nabla N) - \frac{\partial}{\partial E_e} (\dot{E}_e N) + Q \quad (1)$$

where \dot{E}_e is the energy change rate of electron due to synchrotron radiation and IC radiation. Q is the source term depicting the electron injection from the pulsar. \mathcal{D} is the diffusion tensor. For simplicity, we solve the equation in the cylinder coordinate, defining the z -axis to be

the direction of the mean magnetic field and the pulsar location to be the origin. By further assuming the system to be symmetric with respect to the z -axis (i.e., $\partial/\partial\theta = 0$), we can write the transport equation into

$$\frac{\partial N}{\partial t} = \frac{1}{r} \frac{\partial}{\partial r} \left(r D_{rr} \frac{\partial N}{\partial r} \right) + D_{zz} \frac{\partial^2 N}{\partial z^2} - \frac{\partial}{\partial E_e} \left(\dot{E}_e N \right) + Q(E_e) S(t) \delta(r) \delta(z). \quad (2)$$

where the diffusion coefficient parallel to the mean magnetic field and perpendicular to it can be set, respectively, by

$$D_{zz} = D_{\parallel} = D_0 (E_e/1\text{GeV})^q \quad (3)$$

$$D_{rr} = D_{\perp} = D_{zz} M_A^4 \quad (4)$$

Here we neglect the drift effect which would cause asymmetric diffusion, and take D_{\parallel} to be the standard ISM diffusion coefficient throughout the work which is $D_0 = 3.8 \times 10^{28} \text{cm}^2 \text{s}^{-1}$ and $q = 1/3$ [13]. Based on our motivation in this study, we will only look into the case with $M_A = 0.1, 0.2, 0.3$ respectively, since a larger M_A would result in a less anisotropic magnetic field topology. The rightmost term in Eq. 2 consists of three parts: the Dirac functions $\delta(r)$ and $\delta(z)$ specify the injection location, $Q(E_e, t)$ represents the injection spectrum of electron, and $S(t)$ shows the temporal behavior of the injection rate. More specifically, we assume the injection spectrum of electron to follow a power-law distribution $Q(E_e) = N_0 E_e^{-p} e^{E_e/E_{\max}}$, starting from 1 GeV. Here, N_0 is the normalization constant, p is the spectral index and E_{\max} is the high-energy cutoff energy in the spectrum. [4] reported a null detection of the diffuse multi-GeV emission from the vicinity of Geminga by *Fermi*-LAT, suggesting a hard injection spectrum of electron from the PWN. We fix the value of p to be 1.6 in this work, noting that the value of p is actually not important to the predicted X-ray flux as long as the TeV observation is reproduced. E_{\max} is assumed to be 200 TeV to produce a proper spectral shape measured by HAWC under the hard injection spectrum. Assuming the pulsar to be a pure dipole radiator with a braking index of 3, we have $S(t) = (1 + t/\tau)^{-2}$ with $\tau = 12$ kyr being the spin-down timescale of the pulsar. The value of N_0 is then determined by $\int \int S(t) Q(E_e) dE_e dt = W_e$ where W_e is the only free parameter in our model, i.e., the total injected energy in CRe. The evolution of the differential electron density $N(E_e, r, z, t)$ is solved by a finite difference method (see Supplement for details).

Next, we calculate the emissivity of electrons in the Cartesian coordinate system. Again, we put the pulsar at the origin ($x_P = 0, y_P = 0, z_P = 0$) and define the direction of the mean magnetic field as the z -axis. We define the x -axis so that the line connecting the pulsar and the observer, i.e., \overline{PO} , is in the xz plane (see Fig. 1 for a sketch). Then we envisage a random point E in

the space and denote the distance between the point to the observer (i.e., the length of \overline{EO}) by l , and denote the angle between the line \overline{EO} and the line \overline{PO} by θ . Now let us further consider a circle perpendicular to both the xz plane and the line \overline{PO} , with its center, denoted by C , attaching to the line \overline{PO} and with the point E on the ring. The two intersection points of the circle and the xz plane are called point A and B respectively, and we call the angle between the line \overline{AC} and the line \overline{CE} angle ζ . The coordinates of point E can then be given by

$$x_E = (d_{\text{gem}} - l \cos \theta) \sin \phi - l \sin \theta \cos \zeta \cos \phi \quad (5)$$

$$y_E = l \sin \theta \sin \zeta \quad (6)$$

$$z_E = (d_{\text{gem}} - l \cos \theta) \cos \phi + l \sin \theta \cos \zeta \sin \phi \quad (7)$$

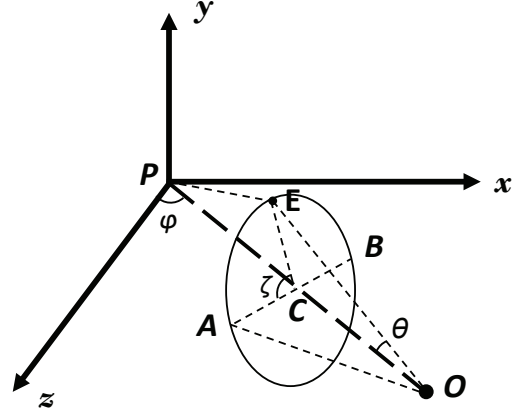


FIG. 1. Sketch figure of the geometry. See text for more details.

The electron density at an arbitrary point E can be found by interpolation given z_E and $r_E = \sqrt{x_E^2 + y_E^2}$, based on the obtained electron density distribution $N(E, z, r)$. The number of electron in the element volume in the neighbourhood of point E can then be given by

$$dN(E, z, r) = N(E, z, r) (l \sin \theta d\zeta \cdot l d\theta \cdot dl) \quad (8)$$

where the quantity in the bracket represents the element volume around E . Note that, although the angular distribution of electron is still isotropic (i.e., $dN/d\Omega = N(E, z, r)/4\pi$ since the mean scattering time of an electron $\sim D/c^2$ is much shorter than the cooling timescale in the energy range of interest in this work), the synchrotron radiation is anisotropic given a mean orientation of magnetic field considered in this work. Due to the relativistic beaming effect, we can only receive the radiation of electrons moving towards us and the radiation power highly depends on the pitch angle α with respect to the local magnetic field. The later one is determined by the viewing angle ϕ and the position of the point E . If there is no magnetic field perturbation, the pitch angle of electrons moving towards us can

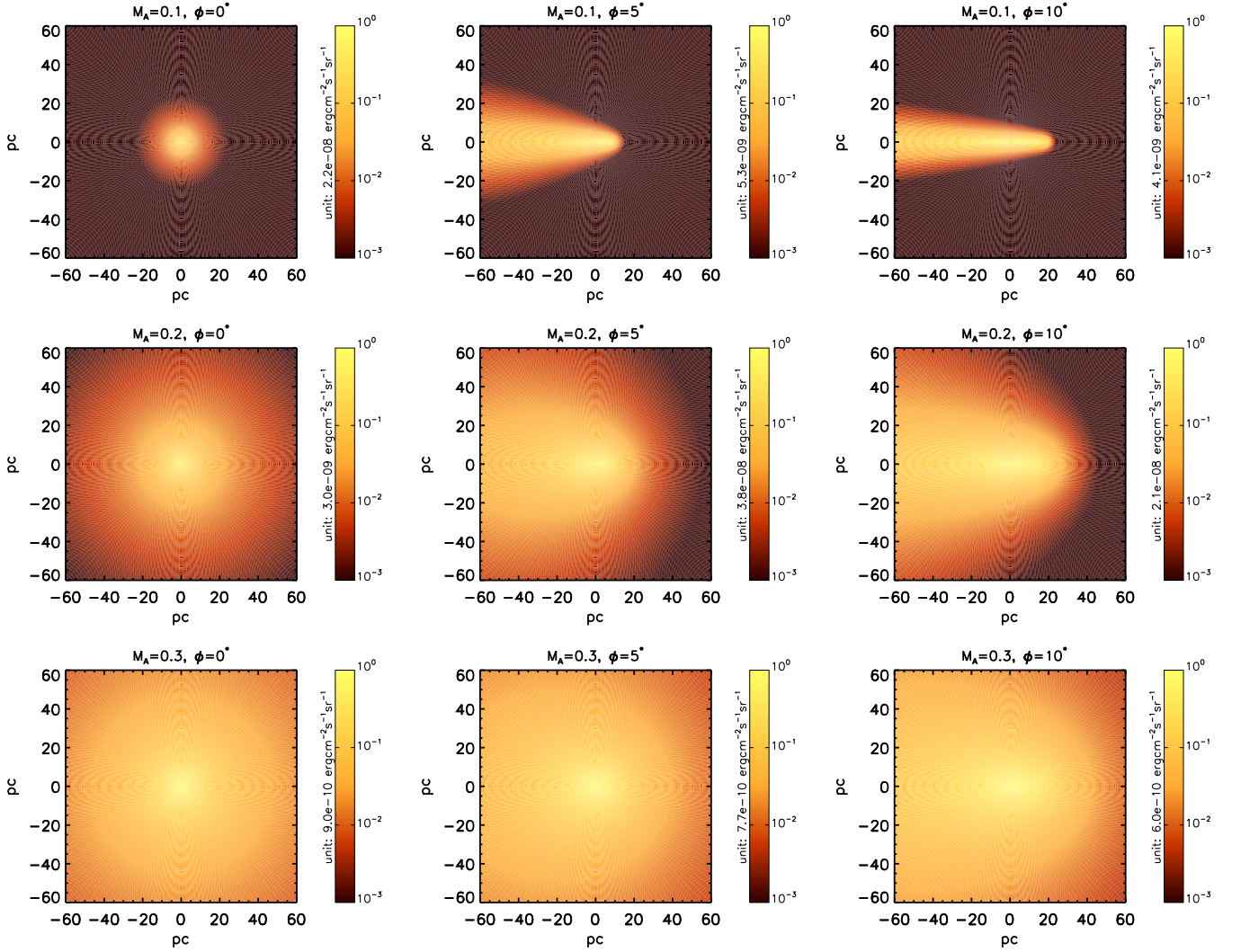


FIG. 2. Predicted 8 – 40 TeV SBP with different Alfvénic Mach number M_A (from top to bottom rows: $M_A = 0.1, 0.2, 0.3$) and different viewing angle ϕ (from left to right columns: $\phi = 0^\circ, 5^\circ, 10^\circ$).

be given by $\cos \alpha_0 \equiv \vec{EO} \cdot \vec{u}_z / \overline{EO} = (z_O - z_E) / l = \cos \theta \cos \phi - \sin \theta \sin \phi \cos \zeta$, where \vec{u}_z is the unit vector along z -axis. In the presence of perturbation, the local magnetic field direction will deviate from the z -axis by an angle δ . The average cosine of the pitch angle then becomes $\cos \alpha = \cos \alpha_0 \cos \delta$. The distribution of $\cos^2 \delta$, i.e., $f(\cos^2 \delta)$, where $\int f(\cos^2 \delta) d \cos^2 \delta = 1$, is obtained from the MHD turbulence simulations [14]. The flux of synchrotron radiation by electrons in the element volume in the neighbourhood of point E can then be given by

$$dF_{\text{syn}}(\epsilon) = \int \mathcal{F}_{\text{syn}} \{dN(E, z, r), B \sin \alpha\} \times f(\cos^2 \delta) d \cos^2 \delta / 4\pi l^2 \quad (9)$$

The IC radiation is isotropic and flux can be given by

$$dF_{\text{IC}}(\epsilon) = \mathcal{F}_{\text{IC}} \{dN(E, z, r), n_{\text{ph}}\} / 4\pi l^2 \quad (10)$$

where n_{ph} is the differential density of the background

photon field. Following [1], in addition to CMB, we also consider the interstellar emission of an infrared photon field (with a temperature of 20 K and an energy density of 0.3 eV), and an optical photon field (with a temperature of 5000 K and an energy density of 0.3 eV).

For observers at Earth, radiation of all the electrons in the LOS add up and is projected onto the celestial sphere. The intensity at any given direction depicted by θ and ζ can then be found by $I(\epsilon, \theta, \zeta) = \int dF / \sin \theta d\theta d\zeta$. More specifically, we can obtain the intensity of synchrotron radiation and the intensity of IC radiation by, respectively,

$$I_{\text{syn}}(\epsilon, \theta, \zeta) = \frac{1}{4\pi} \int_{\cos^2 \delta} \int_{l_{\min}}^{l_{\max}} \mathcal{F}_{\text{syn}} \{N(E, z, r), B_0 \sin \alpha\} \times f(\cos^2 \delta) d \cos^2 \delta dl \quad (11)$$

and

$$I_{\text{IC}}(\epsilon, \theta, \zeta) = \frac{1}{4\pi} \int_{l_{\min}}^{l_{\max}} \mathcal{F}_{\text{IC}} \{N(E, z, r), n_{\text{ph}}\} dl \quad (12)$$

where n_{ph} is the photon number density of the background radiation. The total flux within certain angle θ_0 from the pulsar can be obtained by $F(\epsilon, \theta < \theta_0) = \int_0^{\theta_0} \int_0^{2\pi} I(\epsilon, \theta, \zeta) \sin \theta d\theta d\zeta$, where $I = I_{\text{syn}} + I_{\text{IC}}$.

Result- Employing a typical ISM diffusion coefficient for $D_{\parallel} = 3.8 \times 10^{28} (E/1\text{GeV})^{1/3}$ and a typical ISM magnetic field strength of $B = 3\mu\text{G}$, we firstly show the predicted 8-40 TeV morphology for different Alfvénic mach number M_A and different viewing angle ϕ in Fig. 2. The Geminga pulsar is located at the center of each panel or the coordinate (0,0). The horizontal axis is parallel to the line \overline{AB} while the vertical axis is parallel to y -axis in Fig. 1. The projected distance is calculated based on a nominal distance of 250 pc for Geminga. We can see that the morphology is highly anisotropic in the cases of $\phi = 5^\circ$ with $M_A = 0.1$, and in the case of $\phi = 10^\circ$ with $M_A = 0.1$ and $M_A = 0.2$. In all the cases of $M_A = 0.3$, the resultant morphologies do not show a sufficient gradient as that observed by HAWC. We therefore exclude these cases and focus on the cases of $\phi = 0^\circ$ with $M_A = 0.1$ and 0.2 , and $\phi = 5^\circ$ with $M_A = 0.2$ below.

Since the cooling timescale of multi-TeV-emitting electron/positron is $t_c \lesssim 10^{12}\text{s}$, the perpendicular diffusion length is $2\sqrt{D_{\perp} t_c} < 40\text{ pc}$. Hence, integrating the intensity over a circular region with a radius of 10° centred at Geminga is sufficient. We also integrate the intensity over a circular region with $600''$ radius centered at Geminga to compare the predicted X-ray flux in this region with the Chandra/XMM-Newton upper limit. In the calculation, the only free parameter is the total injection power of electrons/positrons W_e , by adjusting which we normalize the predicted TeV flux to that measured by HAWC. The multiwavelength flux and the surface brightness profiles (SBPs) in these three cases are shown in Fig. 3. As we can see, in all three cases the predicted X-ray fluxes are lower than the upper limit of XMM-Newton (and also Chandra). However, the predicted multi-TeV SBP for $M_A = 0.1$ is too steep. This is because the perpendicular diffusion coefficient is only $D_{\perp} = 3.8 \times 10^{24} (E_e/1\text{GeV})^{1/3} \text{cm}^2\text{s}^{-1}$ for $M_A = 0.1$, and with such a small diffusion coefficient, the perpendicular diffusion distance is only $\sim 5\text{ pc}$ before TeV-emitting electrons cool. For a viewing angle of $\phi = 0^\circ$, such a perpendicular diffusion length is translated to only $\sim 1^\circ$ extension in the celestial sphere. On the other hand, the prediction is in good agreement with observation in the case of $M_A = 0.2$ with $\phi = 0^\circ$. For $M_A = 0.2$ and $\phi = 5^\circ$, the predicted SBP is a little flatter than the observation but still consistent with 2σ error of the data. We therefore conclude that $M_A \simeq 0.2$ with a viewing angle $\lesssim 5^\circ$ is preferable to reproduce the X-ray and TeV observation. Such an interpretation can be tested if future radio

observation on Geminga pulsar can detect its rotation measure and dispersion measure, as we then may estimate the mean field direction by comparing the parallel magnetic field strength inferred from these two measurements to the typical ISM magnetic field strength.

Lastly, we note that given the distance from Geminga to Earth being 250 pc, the intervening ISM is expected to contain two or three coherent magnetic fields. The mean magnetic field is unlikely always aligned with our LOS between Geminga and Earth. The pitch angle between the electron moving towards us and the mean field is supposed to be larger outside the TeV halo. The potential increase of synchrotron radiation flux is, however, limited [15]. Another related issue is the contribution of Geminga to the positron excess measured in many experiments above 10 GeV [16–18]. There is a debate on the contribution of Geminga to the positron excess in the framework of inefficient (isotropic) diffusion of particles [2–4, 19, 20]. In the global frame from Geminga to Earth, the injected positrons from Geminga are likely to diffuse fast with the typical ISM diffusion coefficient so that the resulting positron flux at Earth can reach the level of the positron excess, unless the global mean magnetic field between Geminga and Earth is perpendicular to LOS.

-
- [1] A. U. Abeysekara, A. Albert, R. Alfaro, C. Alvarez, J. D. Álvarez, and et al., *Science* **358**, 911 (2017), 1711.06223.
 - [2] K. Fang, X.-J. Bi, P.-F. Yin, and Q. Yuan, *Astrophys. J.* **863**, 30 (2018), 1803.02640.
 - [3] S. Profumo, J. Reynoso-Cordova, N. Kaaz, and M. Silverman, *Phys. Rev. D* **97**, 123008 (2018), 1803.09731.
 - [4] S.-Q. Xi, R.-Y. Liu, Z.-Q. Huang, K. Fang, H. Yan, and X.-Y. Wang, *ArXiv e-prints* (2018), 1810.10928.
 - [5] R.-Y. Liu, C. Ge, X.-N. Sun, and X.-Y. Wang, *Astrophys. J.* **875**, 2 (2019).
 - [6] R. Kulsrud and W. P. Pearce, *Astrophys. J.* **156**, 445 (1969).
 - [7] A. J. Farmer and P. Goldreich, *Astrophys. J.* **604**, 671 (2004), astro-ph/0311400.
 - [8] H. Yan and A. Lazarian, *Astrophys. J.* **614**, 757 (2004), astro-ph/0408172.
 - [9] A. Lazarian, *Astrophys. J.* **833**, 131 (2016), 1607.02042.
 - [10] K. Fang, X.-J. Bi, and P.-F. Yin, *arXiv e-prints* (2019), 1903.06421.
 - [11] H. Yan and A. Lazarian, *Astrophys. J.* **673**, 942-953 (2008), 0710.2617.
 - [12] S. Xu and H. Yan, *Astrophys. J.* **779**, 140 (2013), 1307.1346.
 - [13] R. Trotta, G. Jóhannesson, I. V. Moskalenko, T. A. Porter, R. Ruiz de Austri, and A. W. Strong, *Astrophys. J.* **729**, 106 (2011), 1011.0037.
 - [14] K. Makwana, H.-R. Yan, submitted
 - [15] Note1, an upper limit of $2\mu\text{G}$ magnetic field is obtained in the extreme case of a mean magnetic field perpendicular to LOS outside the TeV halo.
 - [16] O. Adriani, G. C. Barbarino, G. A. Bazilevskaya, R. Bellotti, M. Boezio, E. A. Bogomolov, L. Bonechi, M. Bongi,

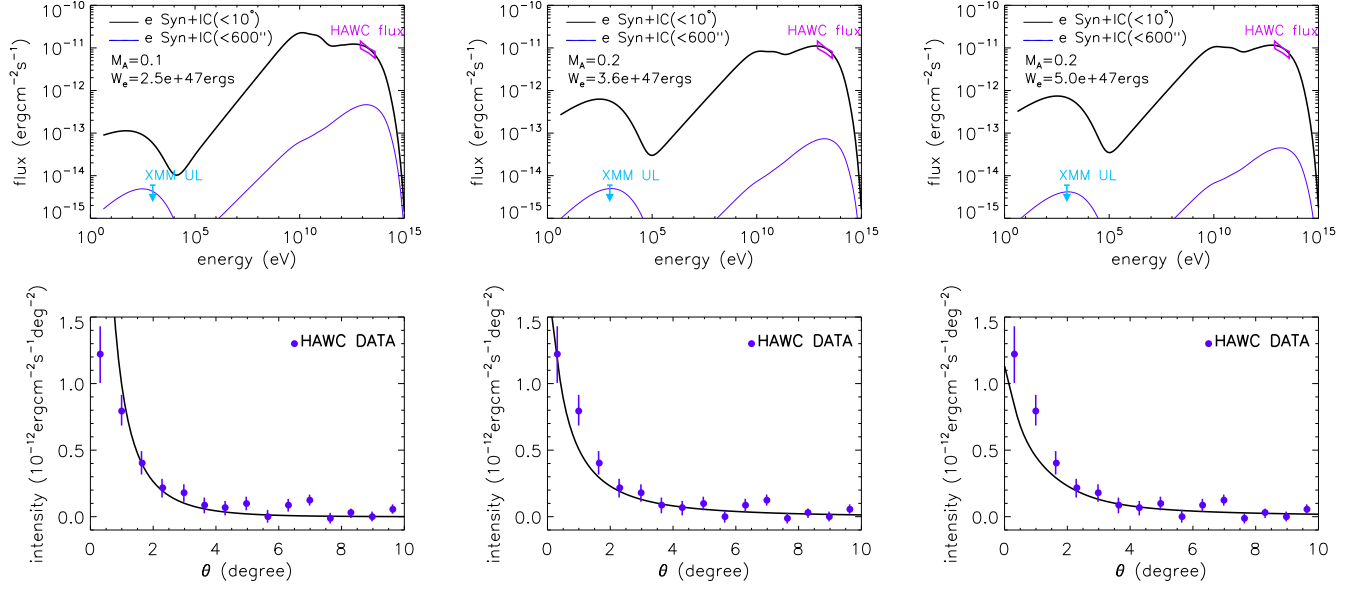


FIG. 3. **Left:** Result in the case of $M_A = 0.1$ and $\phi = 0^\circ$. **Middle:** Result in the case of $M_A = 0.2$ and $\phi = 0^\circ$. **Right:** Result in the case of $M_A = 0.2$ and $\phi = 5^\circ$. Upper panels show the predicted multiwavelength flux from a region within 10° from Geminga (black curve) and from a region within $600''$ from Geminga (blue curve). The magenta bowtie and the cyan arrow represent the flux measured by HAWC and the upper limit from XMM-Newton respectively. Lower panels exhibit the predicted 1D (ϕ -averaged) SBP in 8 – 40 TeV in comparison with the measured one by HAWC, which is shown as blue circles.

- V. Bonvicini, S. Bottai, et al., *Nature (London)* **458**, 607 (2009), 0810.4995.
- [17] M. Ackermann, M. Ajello, A. Allafort, W. B. Atwood, L. Baldini, G. Barbiellini, D. Bastieri, K. Bechtol, R. Bellazzini, B. Berenji, et al., *Physical Review Letters* **108**, 011103 (2012), 1109.0521.
- [18] M. Aguilar, D. Aisa, A. Alvino, G. Ambrosi, K. Andeen, L. Arruda, N. Attig, P. Azzarello, A. Bachlechner, F. Barao, et al., *Physical Review Letters* **113**, 121102 (2014).
- [19] D. Hooper, I. Cholis, T. Linden, and K. Fang, *Phys. Rev. D* **96**, 103013 (2017), 1702.08436.
- [20] X. Tang and T. Piran, *Mon. Not. R. Astron. Soc.* **484**, 3491 (2019), 1808.02445.

SOLVING THE TRANSPORTATION EQUATION

We employ the operator splitting technique to solve Eq. 2, such that the problem can be simplified into solving a convection equation in energy space and a diffusion equation in real space separately. The Strang splitting scheme is used to decouple the energy operator and the spatial operator, with the flow chart as

$$N^l \xrightarrow[(t_l, t_{l+1/2})]{\mathcal{L}_E} \tilde{N}^{l+1/2} \xrightarrow[(t_l, t_{l+1})]{\mathcal{L}_r} N^{l+1/2} \xrightarrow[(t_{l+1/2}, t_{l+1})]{\mathcal{L}_E} N^{l+1}, \quad (13)$$

with l being the index of the time step. The spatial operator \mathcal{L}_r contain both the r -derivative terms and z -derivative terms. We further employ the alternating-direction implicit method to divide each time step into two steps of size $\Delta t/2$, and each step can be solved using tridiagonal matrix algorithm.

The implicit second-order upwind scheme is used to discretize the convection equation in energy space as

$$\frac{N_{i,j,k}^{l+1} - N_{i,j,k}^l}{\Delta t} = \frac{1}{2} \left[\frac{-b_{i,j,k+2}N_{i,j,k+2}^{l+1} + 4b_{i,j,k+1}N_{i,j,k+1}^{l+1} - 3b_{i,j,k}N_{i,j,k}^{l+1}}{2\Delta E} + \frac{-b_{i,j,k+2}N_{i,j,k+2}^l + 4b_{i,j,k+1}N_{i,j,k+1}^l - 3b_{i,j,k}N_{i,j,k}^l}{2\Delta E} \right]. \quad (14)$$

where i and j are the indexes of the spatial step in r direction and z direction respectively, while k is the index of the energy step. The above equation can be reduced into

$$N_{i,j,k}^{l+1} = \left[\frac{-b_{i,j,k+2}N_{i,j,k+2}^{l+1} + 4b_{i,j,k+1}N_{i,j,k+1}^{l+1} - 3b_{i,j,k}N_{i,j,k}^{l+1} - b_{i,j,k+2}N_{i,j,k+2}^l + 4b_{i,j,k+1}N_{i,j,k+1}^l}{4\Delta E} \Delta t + N_{i,j,k}^l \right] / \left[1 + \frac{3b_{i,j,k}\Delta t}{4\Delta E} \right]. \quad (15)$$

Given the boundary condition $N_{i,j,k_{\max}} = 0$ for any l , we can solve $N_{i,j,k}^{l+1}$ from $k = k_{\max} - 1$ to $k = 0$. Note that when adopting the Strang splitting scheme, one should replace Δt by $\Delta t/2$.

To solve the diffusion equation, we first discretize the equation implementing the Crank-Nicolson scheme, and obtain

$$\begin{aligned} \frac{N_{i,j,k}^{l+1} - N_{i,j,k}^l}{\Delta t} &= \frac{D_{rr,k}}{2r_i} \left(\frac{N_{i+1,j,k}^l - N_{i-1,j,k}^l}{2\Delta r} + \frac{N_{i+1,j,k}^{l+1} - N_{i-1,j,k}^{l+1}}{2\Delta r} \right) \\ &+ \frac{D_{rr,k}}{2} \left(\frac{N_{i+1,j,k}^{l+1} - 2N_{i,j,k}^{l+1} + N_{i-1,j,k}^{l+1}}{\Delta r^2} + \frac{N_{i+1,j,k}^l - 2N_{i,j,k}^l + N_{i-1,j,k}^l}{\Delta r^2} \right) \\ &+ \frac{D_{zz,k}}{2} \left(\frac{N_{i,j+1,k}^l - 2N_{i,j,k}^l + N_{i,j-1,k}^l}{\Delta z^2} + \frac{N_{i,j+1,k}^{l+1} - 2N_{i,j,k}^{l+1} + N_{i,j-1,k}^{l+1}}{\Delta z^2} \right) \end{aligned} \quad (16)$$

By applying the ADI method, the above equation can be divided into

$$\begin{aligned} \frac{N_{i,j,k}^{l+1/2} - N_{i,j,k}^l}{\Delta t} &= \frac{D_{rr,k}}{2r_i} \left(\frac{N_{i+1,j,k}^{l+1/2} - N_{i-1,j,k}^{l+1/2}}{2\Delta r} \right) + \frac{D_{rr,k}}{2} \left(\frac{N_{i+1,j,k}^{l+1/2} - 2N_{i,j,k}^{l+1/2} + N_{i-1,j,k}^{l+1/2}}{\Delta r^2} \right) \\ &+ \frac{D_{zz,k}}{2} \left(\frac{N_{i,j+1,k}^l - 2N_{i,j,k}^l + N_{i,j-1,k}^l}{\Delta z^2} \right) \end{aligned} \quad (17)$$

and

$$\begin{aligned} \frac{N_{i,j,k}^{l+1} - N_{i,j,k}^{l+1/2}}{\Delta t} &= \frac{D_{rr,k}}{2r_i} \left(\frac{N_{i+1,j,k}^{l+1/2} - N_{i-1,j,k}^{l+1/2}}{2\Delta r} \right) + \frac{D_{rr,k}}{2} \left(\frac{N_{i+1,j,k}^{l+1/2} - 2N_{i,j,k}^{l+1/2} + N_{i-1,j,k}^{l+1/2}}{\Delta r^2} \right) \\ &+ \frac{D_{zz,k}}{2} \left(\frac{N_{i,j+1,k}^{l+1} - 2N_{i,j,k}^{l+1} + N_{i,j-1,k}^{l+1}}{\Delta z^2} \right) \end{aligned} \quad (18)$$

For the inner boundary condition where $i = 0$ and/or $j = 0$, we utilize the spatial symmetry, i.e., $N_{-1,j,k} = N_{1,j,k}$ and $N_{i,-1,k} = N_{i,1,k}$. We impose the CR density to be 0 at the outer boundary which is set to be $r = 150$ pc and/or $z = 2.5$ kpc.